Theory and computation of photopolymerization-induced phase transition and morphology development in blends of crystalline polymer and photoreactive monomer

Pankaj Rathi and Thein Kyu*
Department of Polymer Engineering, University of Akron, Akron, Ohio 44325, USA
(Received 17 November 2008; published 16 March 2009)

A hypothetical phase diagram of a crystalline polymer/photoreactive monomer mixture has been calculated on the basis of phase field (PF) free energy of crystal solidification in conjunction with Flory-Huggins (FH) free energy of liquid-liquid demixing to guide the morphology development during photopolymerization of poly(ethylene oxide)/triacrylate blend. The self-consistent solution of the combined PF-FH theory exhibits a crystalline-amorphous phase diagram showing the coexistence of solid+liquid gap bound by the liquidus and solidus lines, followed by an upper critical solution temperature at a lower temperature. When photopolymerization was triggered in the isotropic region, i.e., slightly above the crystal melting transition temperatures, the depressed melting transition line moves upward. When it surpasses the reaction temperature, both crystallization and phase separation occur. The temporal evolution of phase morphology is examined in the context of time-dependent Ginzburg-Landau equations coupled with the energy balance (heat conduction) equation using the aforementioned PF-FH free-energy densities. Of particular interest is that the emerged morphology in the crystalline blends depends on the competition between dynamics of liquid-liquid phase separation and/or liquid-solid phase transition (i.e., crystallization) and photopolymerization rates.

DOI: 10.1103/PhysRevE.79.031802 PACS number(s): 61.41.+e

I. INTRODUCTION

Chemical reaction driven phase transition of a polymerizing liquid crystalline system is a nonequilibrium and nonlinear phenomenon involving liquid-liquid phase separation and liquid-crystal (LC) ordering [1–11]. Such phase transitions have been of considerable interest because of their potential use in manufacture of polymer dispersed liquid crystals (PDLCs). For a better control of the droplet dispersion and LC domain morphology, polymerization reaction has been customarily carried out in the isotropic state either by thermal initiation or photoinitiation of the free radical initiators. With the progression of the reaction, the molecular weight of the reactive constituent increases which in turn suppresses blend miscibility between the components, leading to phase separation. There have been several efforts in the literature to theoretically model the phenomenon of liquid-liquid phase separation and mesophase ordering of LC driven by photopolymerization [9–12]. In the blends containing crystalline constituents, phase separation occurs in competition with crystallization [13–16]. Although the polymerization-induced phase separation has been well documented [1–12], the phenomenon of polymerization-induced crystallization in a crystallizing system is novel [13]. More importantly, polymerization-driven phase transition in soft materials such as liquid crystal or crystalline mixtures shares a common ground with the directional solidifications of conventional materials such as metal alloys or ceramics [17–20] and biological excitable media [21].

In a miscible system containing a crystalline polymer and a polymeric solvent, the melting temperature of the polymer crystal is lowered below its pure state value, which may be attributed to the plasticization effect on the crystal melting imposed by the surrounding monomer diluent [22]. Upon polymerization in the isotropic state, the molecular weight of the reactive component increases; this in turn makes the system unstable and therefore triggers liquid-liquid phase separation. Concurrently, the depressed melting temperature of the crystalline constituent tends to restore its pure state value. When the movement of the solid-liquid transition line surpasses the reaction temperature, it drives crystallization; this phenomenon is hereafter termed as polymerization-induced crystallization. Such unique phenomenon of photopolymerization-induced crystallization was reported first by Park *et al.* [13] for a blend of polyethylene oxide (PEO) and diacrylate (DA). Upon photopolymerization of the triacrylate (TA) in the isotropic melt, the depressed melting point of PEO crystals pertaining to the solid-liquid phase diagram moves upward beyond the reaction temperature, thereby causing crystallization of PEO to occur in a manner dependent on reaction conditions such as photocuring temperature, composition, as well as reaction rate. Subsequently, the directional growth behavior of PEO crystals in its blend with DA was demonstrated experimentally as a function of photointensity gradients [13].

Photopolymerization-induced crystallization is similar to thermal-quench-induced crystallization except that in the thermal quenching case the supercooling (i.e., the difference in the crystal-melt transition and the reaction temperature) remains constant, whereas the supercooling keeps increasing in the case of photopolymerization although the reaction was carried out isothermally. Since the thermodynamic force (i.e., supercooling) required for crystallization is created by the elevation of the melting point of the crystalline component with the progression of photoreaction, it is analogous to the nonisothermal slow cooling scenario. Photopolymerization is preferred over thermally initiated radical polymerization because it provides added flexibility in carrying out the photoreaction through control of light intensity. Moreover, various

*Corresponding author: tkyu@uakron.edu

holographic patterns can be created by photolithography through wave interference for memory storage.

The present article describes a theoretical approach to establishing thermodynamic phase diagram of a crystalline polymer/photoreactive monomer mixture using a combined phase field theory of crystal solidification [18,23–26] and Flory-Huggins theory of liquid-liquid demixing [22]. Guided by this phase diagram, the spatiotemporal evolution of the nonequilibrium morphology during photopolymerization has been demonstrated in the context of reaction-diffusion equations based on time-dependent Ginzburg-Landau theory [18] coupled with the photopolymerization kinetics [10] and the heat conduction equation [25]. The emerged morphology in the crystalline PEO/noncrystalline triacrylate blends is discussed in relation to the liquid-liquid phase separation in competition with liquid-solid phase transition driven by photopolymerization.

A. Theoretical scheme

The free energy of a polymer blend containing a crystalline constituent consists of three terms: (i) Flory-Huggins (FH) free energy of liquid-liquid demixing, (ii) phase field free energy of crystallization given by the Landau type double-well potential, and (iii) coupling free energy representing the interaction between amorphous and crystal phases

$$\frac{f(\psi,\phi)}{k_BT} = f_{\text{mixing}} + \phi_1 f_{\text{crystal}} + f_{\text{interaction}}. \tag{1}$$

The FH free energy of mixing for the blend of a thermoplastic with a reactive monomer may be expressed as [22]

$$f_{\text{mixing}} = f(\phi) = \frac{\phi_1 \ln \phi_1}{r_1} + \frac{\phi_2 \ln \phi_2}{r_2} + \chi_{\text{FH}}\phi_1\phi_2, \tag{2}$$

where ϕ_1 and ϕ_2 are volume fractions of the constituents under the incompressibility condition $\phi_1+\phi_2=1$ and $\chi_{\text{FH}}=\chi_{aa}=A+B/T$ is the FH interaction parameter with A being entropic correction and $B=(\chi_c-A)T_c$ in which χ_c is the critical FH interaction parameter at the critical solution temperature T_c. The parameters r_1 and r_2 are the number of statistical segments or the lattice sites occupied by the macromolecule and the reactive monomer, respectively.

The free energy of crystallization in a phase field model is given by a Landau type double-well potential pertaining to the crystal order parameter ψ [18,23]

$$f(\psi) = f_{\text{crystal}} = W\left(\frac{\zeta\zeta_0}{2}\psi^2 - \frac{\zeta+\zeta_0}{3}\psi^3 + \frac{1}{4}\psi^4\right), \tag{3}$$

where W, ζ, and ζ_0 are functions of temperature [24]. The potential well at $\psi=0$ indicates the metastable liquid state and $\psi=\zeta_0$ refers to the stable crystalline state with ζ being the free-energy barrier for the crystal nucleation to overcome. The crystal order parameter, ψ, is defined as $\psi=\ell/\ell^0$, where ℓ is the lamellar thickness and ℓ^0 is that of the perfect crystal and thus their ratio represents the linear crystallinity (i.e., one-dimensional crystallinity) [23]. The solidification potential at a given crystallization temperature, T_x, is $\zeta_0=(T_m^0-T_m)/(T_m^0-T_x)$, where T_m^0 is the equilibrium melting temperature and T_m the crystal melting temperature of the crystalline polymer upon crystallization at T_x [18,23]. The coefficient W representing the solidification hump (barrier) is related to the heat of fusion, ΔH_u as follows [18]:

$$W = \frac{6\Delta H_u}{RT}\left(1-\frac{T}{T_m^0}\right)\left(\frac{1}{2}-\zeta\right)^{-1}, \tag{4}$$

where R is the gas constant and the bracket terms signify correction for the supercooling effects. The free energy of coupling interaction between the crystalline component and the monomer is given as

$$f_{\text{interaction}} = \chi_{ca}\phi_1\phi_2\psi^2, \tag{5}$$

where $\chi_{ca}=B_c\Delta H_u/RT$ is the interaction parameter with $B_c=(1-T_m/T_m^0)/\phi_2$ [23]. The contribution $\phi_1\psi$ represents the bulk crystallinity of the polymer with volume fraction ϕ_1 and the contribution $\phi_2\psi$ is the interaction of the crystals with the amorphous monomer, $\phi_2=\phi_m$; hence the term $f_{\text{interaction}}=\chi_{ca}\phi_1\psi\phi_2\psi$ signifies the free energy of crystalline-amorphous interaction [26]. Thus the local free energy of the blend containing a crystalline polymer and a reactive monomer can be given as

$$f(\psi,\phi) = \frac{\phi_1 \ln \phi_1}{r_1} + \frac{\phi_2 \ln \phi_2}{r_2} + \chi_{aa}\phi_1\phi_2 + W\phi_1\left(\frac{\zeta\zeta_0}{2}\psi^2 - \frac{\zeta+\zeta_0}{3}\psi^3 + \frac{1}{4}\psi^4\right) + \chi_{ca}\phi_1\phi_2\psi^2 \tag{6}$$

Note that, the free energy of crystallization is weighted by the volume fraction of the crystalline polymer ϕ_1 to account for the crystallinity in the blends [26].

B. Construction of the phase diagrams

Prior to calculating the coexistence lines, it is important to first determine the solid-liquid phase transition by minimizing the free energy with respect to the crystal order parameter, ψ,

$$\frac{\partial f}{\partial \psi} = \phi_1 W[\psi^3 - (\zeta+\zeta_0)\psi^2 + \zeta\zeta_0\psi] + 2\chi_{ca}\phi_1\phi_2\psi = 0, \tag{7}$$

which gives the equilibrium values of the crystal order parameter ψ for each composition of the blend ϕ_1. The value of ψ thus obtained is subsequently substituted in the free-energy expression and then the pseudochemical potentials are calculated to determine the coexistent points, i.e., $(\partial f/\partial\phi_1)|_{\phi_1^\alpha} = (\partial f/\partial\phi_1)|_{\phi_1^\beta}$. The detailed procedures for seeking the self-consistent solution for the phase diagram involving the double tangent method can be found elsewhere [23].

C. Free-energy change during photopolymerization

During the course of polymerization, the value of r_2 changes to r_P representing the number of statistical segments

of the emerged polymer under the constraint that $\phi_2=\phi_m+\phi_P$. Assuming that the monomer and the polymer thus formed are miscible and have the same FH interaction parameter with respect to the crystalline counter part, Eq. (2) may be rewritten as

$$f_{\text{mixing}} = f(\phi) = \frac{\phi_1 \ln(\phi_1)}{r_1} + \frac{\phi_m \ln(\phi_m)}{r_2} + \frac{\phi_P \ln(\phi_P)}{r_P} + \chi_{aa}\phi_1(1-\phi_1), \tag{8}$$

assuming that the equilibrium is reached at each conversion. The total free energy of the polymerizing system may be expressed for each conversion step as

$$f(\psi,\phi) = \frac{\phi_1 \ln(\phi_1)}{r_1} + \frac{\phi_m \ln(\phi_m)}{r_2} + \frac{\phi_P \ln(\phi_P)}{r_P} + \chi_{aa}\phi_1(1-\phi_1) + W\phi_1\left(\frac{\zeta\zeta_0}{2}\psi^2 - \frac{\zeta+\zeta_0}{3}\psi^3 + \frac{1}{4}\psi^4\right) + \chi_{ca}\phi_1\phi_m\psi^2. \tag{9}$$

II. PHOTOPOLYMERIZATION KINETICS

The nonequilibrium snapshots of the phase diagram during the course of polymerization reaction were calculated using the instantaneous volume fractions of the monomer and the polymer formed from it, viz.,

$$\alpha = \frac{\phi_2 - \phi_m}{\phi_2}, \quad \phi_P = \alpha\phi_2 \quad \text{or} \quad \phi_m = (1-\alpha)\phi_2, \tag{10}$$

where α is conversion of monomers into a polymer. The rate of conversion is described by the first-order reaction given as

$$\frac{d\alpha}{dt} = k(1-\alpha) = k(\phi_m/\phi_2). \tag{11}$$

In actual photopolymerization, the lumped rate constant k is given as the ratio of the propagation and n power of the termination rate constants, i.e., $k=k_p/k_t^n$, where n is the reaction exponent; it is 0.5 under the assumption of the bimolecular termination reaction between macroradicals [9,12]. The conversion rate is thus proportional to the one-half power of the intensity of irradiation $I_a^{0.5}$ which is valid in the initial stage of the reaction, but at the steady state where termination via trapping is competing with termination by combination, the k value changes according to I_a with $n=1$ [27,28].

A. Dynamic calculations

The total free energy of the blend may be expressed in terms of the local [Eq. (5)] and nonlocal gradient contributions, viz.,

$$F = \int_V \left(f(\phi,\psi) + \frac{\kappa^\phi}{2}|\nabla\phi_k|^2 + \frac{\kappa^\psi}{2}|\nabla\psi|^2 \right) dV, \tag{12}$$

where $\kappa^\phi=\Sigma_{k=1,m,p}a_k^2/18\phi_k$ and κ^ψ are the coefficients of the corresponding interface gradient terms in the composition and crystal-phase order-parameter fields, respectively, and a_k is the characteristic length with subscript $k=1,m,p$ representing crystalline polymer constituent, monomer, and emerging polymer, respectively. The dynamics of the photopolymerization-induced phase transitions may be calculated in the context of time-dependent Ginzburg-Landau (TDGL)-model C by coupling the conserved concentration (or volume fraction, ϕ) and the nonconserved crystal order parameter (ψ). The governing nonlinear reaction-diffusion equations may be described as follows [8–10]:

$$\frac{\partial\phi_1}{\partial t} = \nabla[\Lambda\,\nabla\,(\delta F/\delta\phi_1)] + \eta, \tag{13}$$

$$\frac{\partial\phi_m}{\partial t} = \nabla[\Lambda\,\nabla\,(\delta F/\delta\phi_m)] - \dot{\alpha}\phi_m, \tag{14}$$

$$\frac{\partial\psi}{\partial t} = -\Gamma^\psi\frac{\delta F}{\delta\psi}, \tag{15}$$

where Λ is the mutual diffusion coefficient represented by the Onsager type mobility as $1/\Lambda=(\phi_1/\Lambda_1)+(\phi_m/\Lambda_m)+(\phi_p/\Lambda_p)$ and $\Lambda_k=D_k r_k\phi_k^2$, where D_k is self-diffusion coefficient and r_k is the number of statistical segments. It can be thus anticipated that the mobility changes with changing blend compositions during polymerization. Γ^ψ represents the mobility in the crystal order-parameter field and η indicates the thermal noise that satisfies the fluctuation-dissipation theorem. Equations (13) and (14) are further coupled to the energy conservation equation in what follows:

$$\rho C_P\frac{\partial T}{\partial t} = k_T\nabla^2 T + \Delta H_u\frac{\partial\psi}{\partial t} + \Delta H_P\dot{\alpha}\phi_m, \tag{16}$$

where C_p is heat capacity of the polymer crystal, ρ is density, k_T is thermal conductivity, and ΔH_u is latent heat (or heat of fusion) of the polymer crystal. In addition, ΔH_P is heat of polymerization released during the conversion of the reactive monomer fraction to the polymer. Equations (13)–(15) are simultaneously solved in dimensionless units (signified by the tilde sign) viz., $\tilde{\nabla}=\nabla/a$, $\tilde{t}=tD/a^2$, $\widetilde{\kappa^\psi}=\kappa^\psi/a^2$, and $\widetilde{\Gamma^\psi}=\Gamma^\psi a^2/D$ in conjunction with Eq. (16). The parameters a and D represent the characteristic length and translational diffusion coefficient, respectively.

III. RESULTS AND DISCUSSION

The crystal melting behavior may be analyzed in the framework of a double-well potential of the phase field theory. Figure 1(a) shows the variation of free energy of crystallization of the crystalline polymer with temperature in the absence of monomer. At the equilibrium melting temperature, T_m^0, the free energies of the amorphous melt state ($\psi=0$) and the crystalline state ($\psi=\zeta_0$) are equivalent. When the temperature is raised above T_m^0, the free energy of the melt state is lower than the free energy of the crystalline state. Melting occurs because the amorphous melt state is more stable relative to the metastable crystalline phase. On the other hand at a temperature lower than T_m^0, the crystalline

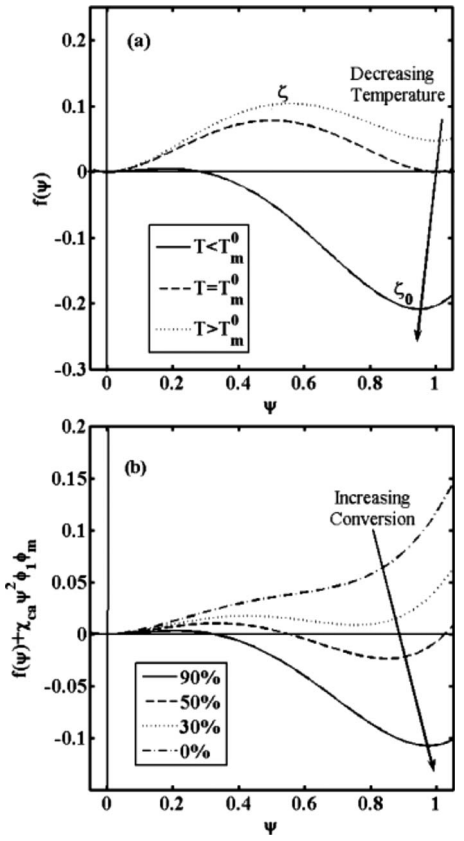

FIG. 1. (a) Free energy of crystallization as a function of temperature showing the equilibrium between liquid and crystalline states at T_m^0; the stable liquid and metastable crystal state at $T>T_m^0$; the metastable melt and the stable crystal state at $T<T_m^0$. (b) Comparison of the free energy of crystallization as a function of conversion showing the lowering of the melting temperature of the crystalline constituent. As the monomer is consumed upon polymerization reaction, the free-energy curve tends to restore toward the pure state.

state at $\psi=\zeta_0$ is stable, as it has a lower free energy than the metastable melt at that temperature and thus crystallization is favored. Figure 1(a) captures the effects of temperature on the free energy of the crystal solidification showing the relative metastable and stable phases depending on whether the temperature is located above or below the melting temperature.

Figure 1(b) shows the variation of the free-energy curves of the crystalline polymer/monomer blends by taking into account the local free energy and the crystal-monomer interaction ($\chi_{ca}\phi_1\phi_m\psi^2$) between the crystalline constituent and the monomer. Note that the free-energy curves in this figure were computed for a reaction temperature of $T_r=323$ K. Although it is below the melting temperature of the pure polymer crystal ($T_m=338$ K), this reaction temperature corresponds to the isotropic state due to the melting point depression occurring in the crystal/monomer blend. As depicted in the 0% conversion curve, the free-energy well of the crystalline state is located above that of the melt state and thus it represents the isotropic melt. Upon exposure to light, the monomer gets converted to a polymer and/or a network, thereby raising the molecular weight of the reactive component, which in turn makes the system to become unstable. This unfavorable crystal-monomer interaction (i.e., reduction in $\chi_{ca}\phi_1\phi_m\psi^2$) pushes the depressed melting temperature of the blends back to the original value of the neat crystalline constituent. As evident in Fig. 1(b), the solidification potential of the free-energy curve decreases with increasing conversion, which in turn raises the supercooling (i.e., the difference between the reaction point and the melting temperature) and eventually drives crystallization. The shift of the free-energy minimum to a larger ψ value implies the increasing trend of linear crystallinity (or crystal perfection) in the blend, demonstrating how crystallization can occur with the progression of the reaction.

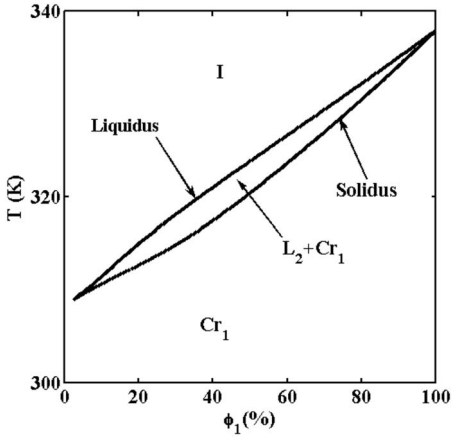

FIG. 2. Phase diagram showing the coexistence of crystal +melt gap bound by the liquidus and solidus lines in comparison with the experimental data of the PEO/TA blend, showing the isotropic single phase (i), solid crystal (Cr_1)+liquid(L_2) coexistence gap bound by the liquidus and solidus lines, and the solvated crystal (Cr_1) region. The parameters used were $r_1=110$, $r_m=2$, $T_m=338$ K, $\chi_{ca}=0.203$, and $\chi_{aa}=0.0134$ at $T=323$ K. The diamond symbols are the experimental data of PEO/TA blends from Ref. [29].

Figure 2 exhibits the calculated phase diagram corresponding to that of PEO/TA blends [29]. The equilibrium phase diagram for this blend was self-consistently solved in accordance with Eq. (6). Various parameters used in the calculation of the phase diagram were $r_1=110$, $r_m=2$, $T_m=338$ K, $\chi_{ca}=0.203$, and $\chi_{aa}=0.0134$ at $T_r=323$ K, obtained from the material parameters and the experimental conditions of the PEO/TA system. The calculated phase diagram reveals the isotropic single phase (I), crystal (Cr_1) +liquid (L_2) coexistence gap bound by the liquidus and solidus lines, and the solvated crystal (Cr_1) [29].

Next, the photoreaction was carried out in the isotropic melt state at a temperature slightly above the melting temperature of the crystalline polymer in the blend. In the free-radical photopolymerization of multiarm functional monomers such as the present TA, it is likely to have a distribution of molecular weights. In addition, network formation would further complicate the evaluation of "r_p" value. Hence, we simply assumed that the number of statistical segments of the emerging polymer r_p may be expressed in term of the average value of the reacted species at each conversion, excluding the residual unreacted monomers, which is given by

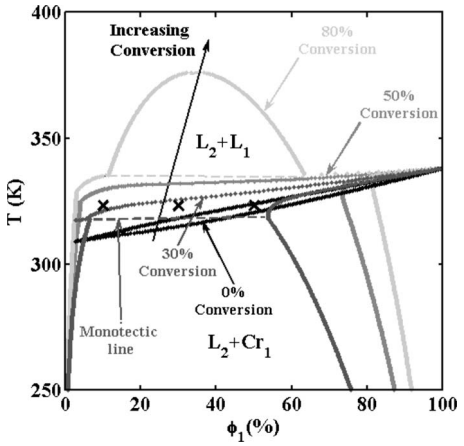

FIG. 3. Evolution of the snapshot phase diagrams showing the rise of L_1+L_2 coexistence envelope corresponding to the phase separated PEO and TA, respectively, followed by straightening of the melting point curve of PEO crystals (Cr_1) with increasing conversion. The symbol Cr_1+L_2 indicates the coexistence of PEO crystals and TA amorphous phase. The dynamic calculations of photopolymerization-induced phase transitions were carried out at the reaction conditions indicated by "×" in the phase diagram. The parameters used were the same as in Fig. 2 with the lumped conversion rate constant of $k=0.1$.

"r_m." As shown in Fig. 3, the $\phi_1=10\%$ and $\phi_1=30\%$ blends at the reaction temperature (indicated by "×" on the phase diagram) were in the isotropic melt state. When the reaction proceeded, the TA monomers were converted into the polymer network. The entropy of the system therefore decreases, thereby pushing up the upper critical solution temperature (UCST) envelope to a higher temperature. Concurrently, this UCST maximum shifts toward the pure crystalline axis while the solid-liquid coexistence gap opens up. When the UCST protrudes above the reaction temperature at high conversions, the phase diagram shows the L_1+L_2 region representing liquid-liquid phase separation overlapping with the Cr_1+L_2 coexistence regions due to crystallization of PEO. The temporal evolution of the snapshot coexistence curves were computed by self-consistently solving the free-energy functional of Eq. (9), assuming that equilibrium is reached at each conversion as depicted in Fig. 3. It can be noticed that the melting point depression curve of the crystalline constituent moves up and concurrently it straightens up with increasing monomer conversion. This elevation of the originally depressed melting point occurs because the crystalline-monomer interaction ($\chi_{ca}\phi_1\phi_m\psi^2$) keeps decreasing with rising molecular weight of the reactive components in the blend. It should be noted that these snapshot phase diagrams are difficult to obtain experimentally, since the actual system may not reach true equilibrium.

The pattern forming aspects of liquid-liquid and liquid-crystal transitions induced by photopolymerization were investigated at three different compositions: $\phi_1=10\%$, $\phi_1=30\%$, and $\phi_1=50\%$ at a reaction temperature of $T_r=323$ K; indicated by × in the phase diagram in Fig. 3. The calculation was performed by solving numerically a set of the nonequilibrium reaction-diffusion equations [i.e., Eqs. (13)–(16)] using a finite difference method with a central difference scheme in the spatial step and the explicit method in the temporal step with a periodic boundary condition on the 500×500 square grid corresponding to the $500\mu\times500\mu$ size. In these calculations, nuclei were randomly created in the crystal order-parameter field along with random white noise in the entire compositional order-parameter field. The dimensionless parameters used in the dynamical calculations were $\tilde{\kappa}^{\psi}=0.35$, $\tilde{\Gamma}^{\psi}=10$, $\tilde{\theta}=3.15$, and $\tilde{K}=1.35$, which were computed from materials parameters including thermal conductivity of PEO, $k_T=0.25$ J/(m s K), density of PEO $\rho=1.2$ g/cm^3, $R=8.314$ J/(K mol), and heat of polymerization for the acrylate monomer $\Delta H_P=86.25$ kJ/mol [26], along with the characteristic length, $a=1$ μm, and translational diffusion coefficient, $D=10^{-12}$ m^2/s.

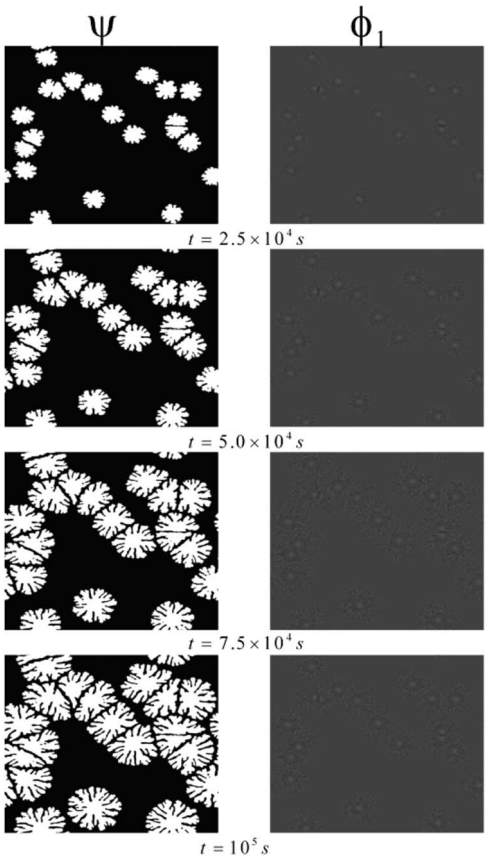

FIG. 4. Spatiotemporal evolution of spherulites in the crystal order (left column) and composition order parameter (right column) at $\phi_1=30\%$ and $T_r=323$ K. The dimensionless parameters used in the dynamical calculations by solving the set of nonlinear reaction-diffusion equations were $\tilde{\kappa}^{\psi}=0.35$, $\tilde{\Gamma}^{\psi}=10$, $\tilde{\theta}=3.15$, and $\tilde{K}=1.35$, which were computed from the materials parameters such as thermal conductivity of PEO, $k_T=0.25$ J/(m s K), density of PEO $\rho=1.2$ g/cm^3, $R=8.314$ J/(K mol), and heat of polymerization for the acrylate monomer $\Delta H_P=86.25$ kJ/mol [26], along with the characteristic length, $a=1$ μm, and translational diffusion coefficient, $D=10^{-12}$ m^2/s. The lumped conversion rate constant was $k=0.1$ at $T_r=323$ K.

Figure 4 shows the temporal evolution of the spherulitic morphology pertaining to the crystal order parameter (left column) and the corresponding compositional order parameter (right column) during the course of photopolymerization

at $T_r=323$ K and $\phi_1=30\%$ under a slow reaction rate of $k=0.1$. At $T_r=323$ K, the initial blend was practically in the isotropic melt state (i.e., the single phase). With the progression of photopolymerization reaction, the monomer gets consumed and its interaction with the crystalline counterpart starts to diminish. This reduced blend miscibility raises the melting temperature of the crystalline component. When the reaction reaches the 30% conversion, the melting point of the crystalline constituent surpasses the reaction temperature, which in turn triggers crystallization. With elapsed time, the crystal growth occurs through branching and tip splitting toward the surrounding melt. In the concentration field, tiny liquid-liquid phase-separated domains are discernible in the branching interlamellar regions as well as in the background melt, implying that liquid-liquid phase separation has occurred in competition with the crystallization of PEO constituent. With elapsed reaction time, the emerging spherulites eventually impinge onto each other. More importantly, these spherulitic entities coexist with the surrounding melt, suggestive of the crystal (solid)-melt (liquid) phase separation.

Under the comparable conditions, the dynamic calculation at the composition of $\phi_1=10\%$ revealed that the system was still in the single phase at the 30% conversion (please see the phase diagram of Fig. 3). Unless sufficient monomer gets converted to polymer, e.g., the 50% conversion curve, the crystal nuclei that were created initially may have dissolved back to the isotropic state. Only when the melting point of the polymerizing blend is elevated above the reaction temperature after sufficient conversion of the monomer into polymer, crystallization can be discerned [Fig. 5(a)]. It is noticed that the emerged spherulitic textures are more disordered with the lamellar branching and splitting being indistinctive relative to the case of $\phi_1=30\%$ blend. In the background, the surrounding melt appears to be isotropic without any indication of liquid-liquid phase separation [Fig. 5(a)]. Another dynamic calculation at $\phi_1=2\%$ concentration neither shows the development of crystalline structure nor liquid-liquid phase separated domains at such low concentration (data not shown). At the 50% conversion, the 10/90 PEO/TA composition is in the metastable gap of the snapshot UCST, and thus if liquid-liquid phase separation were to take place, it has to go through the nucleation and growth (NG) mechanism. Since a higher energy is required for the nucleation (NG) to occur, the fluctuation can decay back to the isotropic state under the present slow polymerization conditions. Moreover, the thermodynamic driving force (i.e., the difference between the reaction temperature and the coexistence point of the snapshot UCST) for the liquid-liquid phase separation is relatively small as compared to that of the $\phi_1=30\%$ case and thus it presents less influence to the emerged spherulitic morphology.

The competition between the liquid-liquid phase separation and the crystallization may be seen more clearly in the higher crystallizable contents. Figures 5(a)–5(c) show the comparison among the emerged crystal morphologies at three reaction conditions denoted by the × marks on the phase diagram corresponding to the 10%, 30%, and 50% crystallizable components of Fig. 3. It can be clearly seen that the crystal-growth rate in the bends containing a higher concentration of the crystalline component, e.g., $\phi_1=50\%$

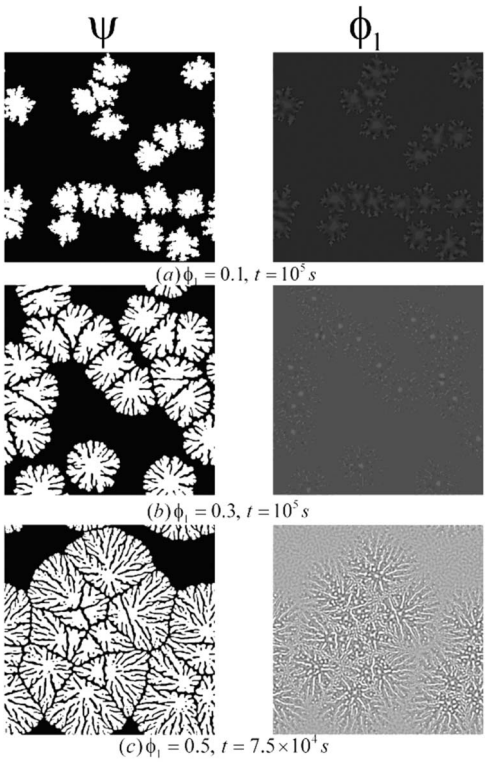

FIG. 5. Emerged spherulitic morphology in competition with liquid-liquid phase separation as a function of composition, exhibiting a faster crystal growth at a higher concentration of the crystalline component. The conversion lumped rate constant was $k=0.1$ at $T_r=323$ K.

[Fig. 5(c)], is faster and the average spherulite size is larger than those of $\phi_1=30\%$ and $\phi_1=10\%$ blends [Figs. 5(b) and 5(a)]. This finding is not surprising in view of the fact that the supercooling is the largest for the 50% PEO as compared to the 30% or 10% compositions due to the depression of the melting point with increasing TA diluent (see Fig. 3). More importantly, at the $\phi_1=50\%$ composition, there is some signature of liquid-liquid phase separation occurring in the background of the concentration order field as well as in the branched interlamellar regions. This observation may be attributed to the crystallization of PEO in the continuum of the liquid-liquid phase separated PEO/TA blend.

The increasingly competitive trend of liquid-liquid phase separation is more recognizable at a higher photopolymerization rate of $k=0.2$ of the $\phi_1=50\%$ case. As can be seen in Fig. 6, the liquid-liquid phase separation via spinodal decomposition has occurred concurrently with crystallization. At the comparable reaction time [compare Fig. 6(a) vs Fig. 6(b)], the emerged spherulite size is smaller and the texture is more disordered, suggesting a slower crystal growth for the faster polymerizing system. Moreover, the bicontinuous spinodal-like domains can be seen in the entire background as well as in the interlamellar region or at the growing lamellar tips, causing the deterioration of the spherulitic texture as evident in the concentration field (Fig. 6). Another plausible account is that the heat of polymerization thus released in combination with the latent (exothermic) heat at the crystal-melt interface may have melted the crystal front locally,

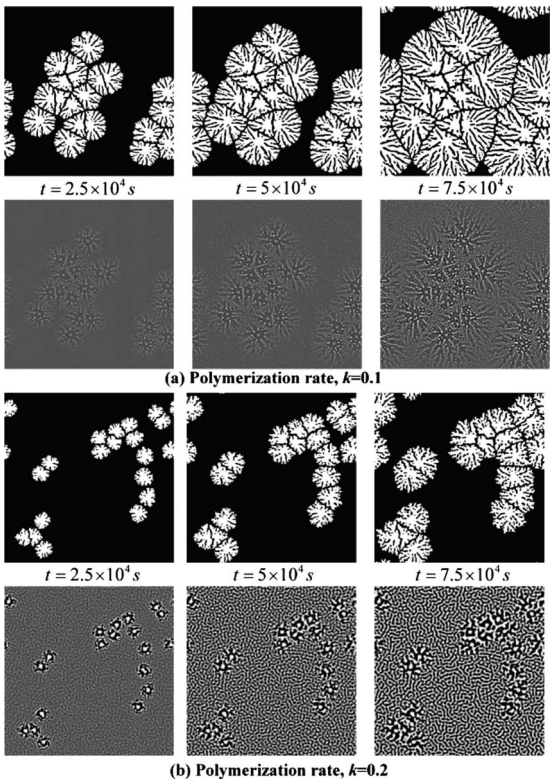

FIG. 6. Morphology evolution in a blend undergoing photopolymerization as a function of polymerization rates of the 50% blends: (a) crystal order parameter in the upper row and composition in the lower row at a lumped conversion rate constant of $k=0.1$ and (b) the corresponding crystal growth at $k=0.2$, showing the hampering influence of liquid-liquid phase separation on the crystal growth.

thereby retarding the crystal growth and also distorting the crystal shapes. Physically, the liquid-liquid phase separation has led to accumulation of the amorphous materials at the growing lamellar fronts, thereby hampering the growth of lamellar crystals. Moreover, the temperature at the local points may have risen due to the heat of polymerization approaching the monotectic line representing the triple coexistence line of the liquid+liquid+crystal phases. It is reasonable to infer that the liquid-liquid phase separation is dominant over the crystallization in the fast polymerizing case and vice versa. Of particular importance is the role of thermal transport involving the heat source such as latent heat of crystallization and heat of polymerization in the crystal-growth dynamics, which should be of interest to a broader area of nonequilibrium and nonlinear dynamics of excitable biological media or chemical systems [21,30] as well as polymer dispersed liquid crystals and photonic crystals [11,12].

IV. SUMMARY

The morphology development in relation to photopolymerization-induced crystallization in the polymerizing crystalline blend has been demonstrated based on the reaction-diffusion equations. In the model, the phase field theory of crystallization coupled with the FH theory of liquid-liquid demixing was successfully used for establishing the phase diagram of the starting mixture and in deciphering the evolution of the snapshot phase diagrams during the course of reaction. The numerical computation based on these coupled time-evolution equations (TDGL model C) with the reaction kinetics and the heat balance equations revealed the spatiotemporal development of the phase morphology, which is dependent on the competition between the liquid-liquid phase separation between PEO/TA pairs and the growth of PEO crystals. It was found that the spherulitic morphology was smaller and more disordered for the faster polymerizing system due to the greater domination by the liquid-liquid phase separation and the polymerization heat released at the propagating lamellar fronts.

ACKNOWLEDGMENT

Support of this work by the National Science Foundation through Grant No. DMR 0514942 is gratefully acknowledged.

[1] J. Y. Kim, C. H. Cho, P. Palffy-Muhoray, M. Mustafa, and T. Kyu, Phys. Rev. Lett. **71**, 2232 (1993).
[2] T. Kyu and J. H. Lee, Phys. Rev. Lett. **76**, 3746 (1996).
[3] E. Girard-Reydet, H. Sautereau, J. Pascault, P. Keates, P. Navard, G. Thollet, and G. Vigier, Polymer **39**, 2269 (1998).
[4] S. Goossens, B. Goderis, and G. Groeninckx, Macromolecules **39**, 2953 (2006).
[5] X. Y. Wang, Y.-K. Yu, and P. L. Taylor, J. Appl. Phys. **80**, 3285 (1996).
[6] H. M. Boots, J. G. Kloosterboer, G. Serbutoviez, and F. J. Touwslager, Macromolecules **29**, 7683 (1996).
[7] J. C. Lee, Phys. Rev. E **60**, 1930 (1999).
[8] D. Nwabunma, H.-W. Chiu, and T. Kyu, J. Chem. Phys. **113**, 6429 (2000).
[9] T. Kyu and D. Nwabunma, Macromolecules **34**, 9168 (2001).
[10] T. Kyu and H.-W. Chiu, Polymer **42**, 9173 (2001).
[11] V. P. Tondiglia, L. V. Natarajan, S. L. Sutherland, D. Tomlin, and T. J. Bunning, Adv. Mater. (Weinheim, Ger.) **14**, 187 (2002).
[12] S. Meng, T. Kyu, L. V. Natarajan, V. P. Tondiglia, R. L. Sutherland, and T. J. Bunning, Macromolecules **38**, 4844 (2005).
[13] S. J. Park, P. Rathi, and T. Kyu, Phys. Rev. E **75**, 051804 (2007).
[14] H. Tanaka and T. Nishi, Phys. Rev. Lett. **55**, 1102 (1985).
[15] H. Tanaka and T. Nishi, Phys. Rev. A **39**, 783 (1989).
[16] H. Wang, K. Shimizu, E. K. Hobbie, Z.-G. Wang, J. C. Meredith, A. Karim, E. J. Amis, B. S. Hsiao, E. T. Hsieh, and C. C. Han, Macromolecules **35**, 1072 (2002).
[17] G. Caginalp and P. C. Fife, Phys. Rev. B **33**, 7792 (1986).
[18] R. Kobayashi, Physica D **63**, 410 (1993).

[19] S. Akamatsu, G. Faivre, and T. Ihle, Phys. Rev. E **51**, 4751 (1995).
[20] V. Ferreiro, J. F. Douglas, J. A. Warren, and A. R. Karim, Phys. Rev. E **65**, 042802 (2002).
[21] *Nonlinear Wave Processes in Excitable Media*, edited by A. V. Holden, M. Marcus, and H. G. Othmer (Plenum, New York, 1991).
[22] P. J. Flory, *Principles of Polymer Chemistry* (Cornell University Press, Ithaca, NY, 1953).
[23] T. Kyu, R. Mehta, and H. W. Chiu, Phys. Rev. E **61**, 4161 (2000).
[24] H. Xu, R. Matkar, and T. Kyu, Phys. Rev. E **72**, 011804 (2005).
[25] H. Xu, W. Keawwattana, and T. Kyu, J. Chem. Phys. **123**, 124908 (2005).
[26] R. Matkar and T. Kyu, J. Phys. Chem. B **110**, 12728 (2006).
[27] C. Decker and K. Moussa, Makromol. Chem. **189**, 2381 (1988).
[28] H. Duran, S. Meng, N. Kim, J. Hu, T. Kyu, L. V. Natarajan, V. P. Tondiglia, and T. J. Bunning, Polymer **49**, 534 (2008).
[29] S. J. Park and T. Kyu, J. Chem. Phys. **129**, 244901 (2008).
[30] R. J. Field and M. Burger, *Oscillations and Traveling Waves in Chemical Systems* (Wiley, New York, 1984).